Astron. Astrophys. 271, 564–573 (1993)

ASTRONOMY AND ASTROPHYSICS

New Herbig-Haro objects and pre-main sequence stars in the star formation region NGC 7129

L. F. Miranda [1], C. Eiroa [2], and A. I. Gómez de Castro [3]

[1] Departamento de Astrofísica, Facultad de Ciencias Físicas, Universidad Complutense de Madrid, E-28040 Madrid, Spain
[2] Departamento de Física Teórica, C-XI, Facultad de Ciencias, Universidad Autonóma de Madrid, Ciudad Universitaria de Cantoblanco, E-28049 Madrid, Spain
[3] ESA-IUE Observatory, Villafranca Satellite Tracking Station, P.O. Box 50727, 28080 Madrid, Spain

Received August 6, accepted October 27, 1992

Abstract. We present CCD images of the central part of the star forming region NGC 7129 as well as spectra of moderate spectral and high spatial resolution of some nebular objects and stars. The images show many reflection filaments which seem to trace the edges of the molecular cavity associated with the pre-main-sequence star LkHα 234. Three new T Tauri-like stars and five new Herbig-Haro (HH) objects have been identified in the region. One of the new young stars probably illuminates an elongated reflection filament. One of the HH objects presents a highly collimated structure and an abrupt and unusually large bending of $\approx 90°$. The object emanates from the Hα-emission line star HL 14. Our spectra indicate that this star is likely to be a T Tauri-like star. Large and systematic variations of the radial velocity, electron density, excitation degree and velocity dispersion exist in the object. The data favor the idea that the object is a jet-like outflow which encounters an obstacle – density enhancement or pressure gradient – in the cloud and deflects. The obstacle could be related to the walls of the molecular cavity associated with LkHα 234 or to the energetic wind from this star.

Key words: reflection nebulae: individual: NGC 7129 – interstellar medium: kinematics and dynamics of – interstellar medium: jets and outflows – stars: pre-main-sequence – stars: mass loss

1. Introduction

NGC 7129 is a star formation region located at a distance of 1 kpc (Racine 1968) in which a cluster of stars in their first evolutionary stages is found (Herbig 1960). The outflow activity is very complex (Hartigan & Lada 1985, hereafter HL). At least two CO outflows are observed (Edwards & Snell 1983). Both are associated with far-IR sources (Bechis et al. 1978; Harvey et al. 1984), NH_3 cloudlets (Güsten & Marcaide 1986), and H_2O masers (Cesarsky et al. 1978; Rodríguez et al. 1980; Sandell & Olofsson 1981). The Herbig Ae/Be star LkHα 234 is the powering source of one of these CO outflows. Dent et al. (1989) found a dust ring around the star and Ray et al. (1990) discovered a jet associated with LkHα 234. A cavity in the ambient CO gas was detected by Bertout, Cabrit and Thum (see Bertout 1987). The cavity is also noticeable in optical photographs where it shows in part as the NGC 7129 reflection nebula. Bertout suggests a causal connection between the stellar wind from LkHα234 and the cloud cavity. Many HH objects are observed in NGC 7129 (Eiroa et al. 1992 and references therein). Three of them, GGD 34, GGD 35 and HH 105, as well as the peculiar object GGD 33 (Goodrich 1986), are seen projected against the redshifted lobe of the CO outflow associated with LkHα 234. The rest of the HH objects, including GGD 32 and HH 103, together with many filament-like nebulous structures are embedded in a diffuse nebulosity located at the southwestern end of the cloud cavity. These HH objects and nebulous structures coincide with blueshifted CO emission (Eiroa et al. 1992).

In this paper we present new CCD images of the central part of NGC 7129. These images show several reflection filaments oriented along the boundaries of the CO cavity and some new HH objects; one of them is interpreted as a strongly bent HH-jet emerging from star 14 in the NGC 7129S field by HL. Hereafter, this star is referred to as HL 14. We also present optical spectra of this object and of some stars in NGC 7129. The spectra allow us to identify

Send offprint requests to: L. F. Miranda

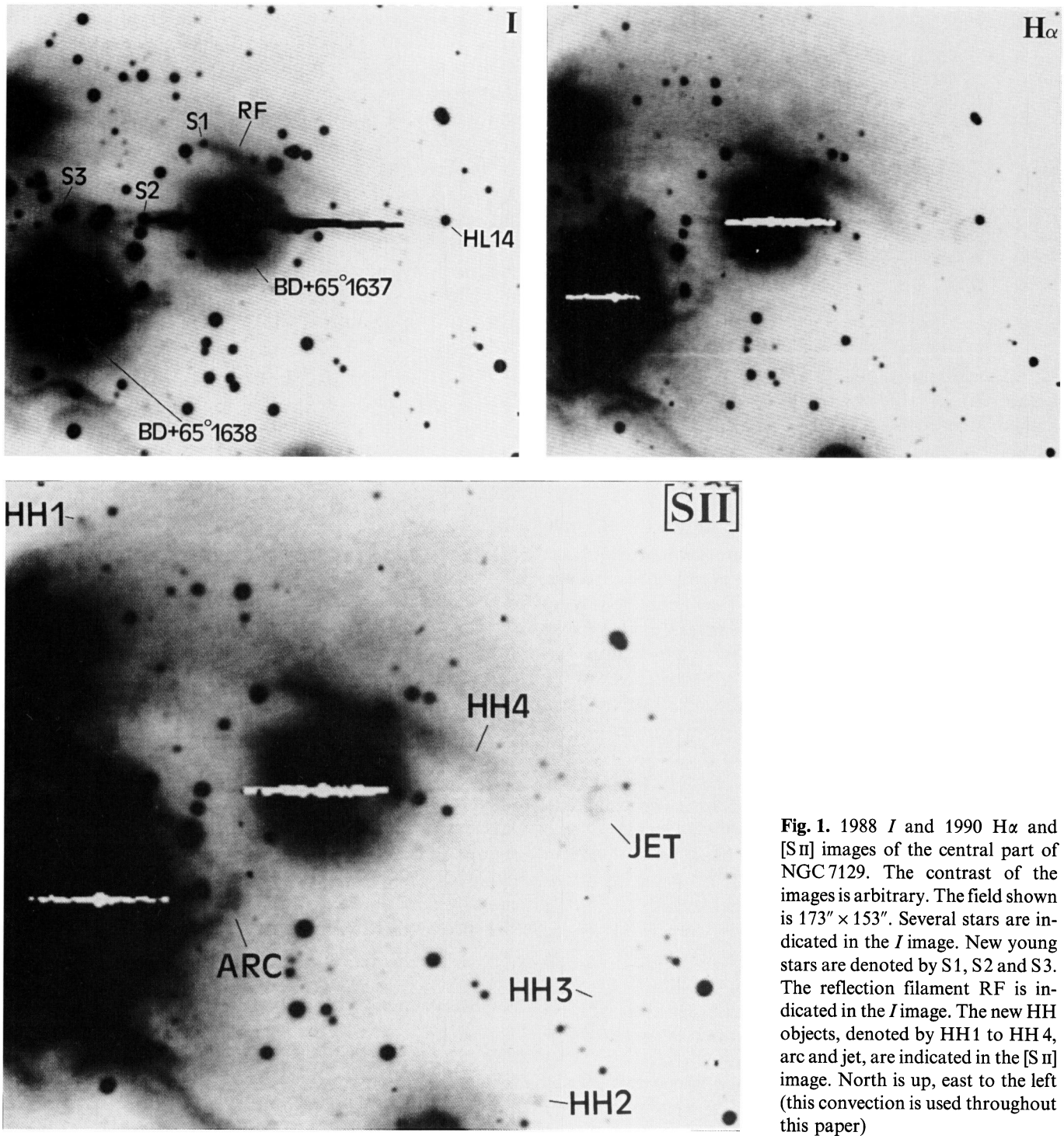

Fig. 1. 1988 *I* and 1990 Hα and [S II] images of the central part of NGC 7129. The contrast of the images is arbitrary. The field shown is 173″ × 153″. Several stars are indicated in the *I* image. New young stars are denoted by S1, S2 and S3. The reflection filament RF is indicated in the *I* image. The new HH objects, denoted by HH1 to HH 4, arc and jet, are indicated in the [S II] image. North is up, east to the left (this convection is used throughout this paper)

several new young stars and also show HH emission at two additional positions.

2. Observations and results

2.1. CCD imaging

CCD images of the central part of NGC 7129 were obtained in July 1988 and October 1990 at the prime focus of the 3.5 m telescope on the Calar Alto Observatory. A RCA CCD with 1024 × 640 pixels of 15 μm in size was used. The scale on the focal plane is 0″.254/pixel and the field of view 260″ × 162″. In 1988 three filters were used: a broad band filter RG 830 (*I* band, $\lambda \approx 9000$ Å) and two narrow band filters Hα ($\lambda \approx 6580$ Å, FWHM ≈ 100 Å) and [S II] ($\lambda \approx 6740$ Å, FWHM ≈ 70 Å). This combination of filters allows us to distinguish between reflected light and shock-excited emission, even though in the *I* band a few faint

Table 1. Coordinates of young stars and HH objects in NGC 7129

Object	α (1950.0)	δ (1950.0)
Star 1	$21^h41^m42^s.7$	65°53′14″
Star 2	21 41 45.8	65 52 50
Star 3	21 41 50.2	65 52 51
HL 14	21 41 29.9	65 52 50
NGC 7129/HH 1	21 41 50.2	65 53 52
NGC 7129/HH 2	21 41 33.3	65 51 37
NGC 7129/HH 3	21 41 31.4	65 51 55
NGC 7129/HH 4	21 41 35.2	65 52 51

HH emission lines are present (e.g. HL; Reipurth & Graham 1988). In addition, the *I* filter can detect light from highly reddened stars. In 1990, new images were obtained using the Hα and [S II] filters only. The seeing was ≈1″.8 in 1988 and 1990. The observations were bias-corrected and flat-fielded using standard procedures.

Figure 1 shows a reproduction of the 1988 *I* and 1990 Hα and [S II] images. Many red stars are distinguished in the *I* image. A large reflection nebulosity is seen encompassing the brightest stars. Structuring this diffuse nebulosity, there is a large number of reflection filaments with curved shapes, which tend to be oriented towards the southwest. These filaments delineate quite well the boundaries of the CO cavity (Bertout 1987). In fact, the nebulosity and the filaments together with the nebulosity and filaments detected in the GGD 32/HH 103 field by Eiroa et al. (1992) completely surround the CO cavity. A hole exists in the central part of the nebulosity. This is more clearly distinguished in the [S II] image. In Hα, the hole is partly covered with very faint nebulosity which could be Hα emission from young stars in the field scattered off by the walls of the cavity. Among the many morphological details seen in the CCD images, we note the existence of two new HH knots, denoted by NGC 7129/HH 1 and NGC 7129/HH 2 in Fig. 1, a curved HH object departing from the star HL 14, and a reflection filament located to the north of star BD +65°1637, denoted by RF, which arises from an extremely red star (hereafter Star 1). Another possible HH object is the arc westwards of BD+65°1638. The arc is clearly observed in Hα and [S II] but is hard to recognize in the *I* image. Coordinates of these objects – except the arc – are given in Table 1, and have been estimated from field stars whose positions are given by Strom et al. (1986). A discussion on RF and on the curved HH object is given below.

2.2. *Spectroscopy*

Long-slit spectra of the curved HH object and RF were obtained in August 1989 at the red channel of the Cassegrain Twin Spectrograph of the 3.5 m telescope. A GEC CCD with 580 × 410 pixels of 17 μm in size was used as detector. The spectra cover the range 6470–6820 Å at a dispersion of 36 Å mm^{-1}. The slit length is 240″. In the case of the curved HH object, two slit positions were used: one centered on HL 14 and oriented at position angle (PA) −90° (hereafter slit **a**), and one centered 8″ to the east of HL 14 and oriented at PA 0° (slit **b**). In the case of RF, the slit was centered on Star 1 and oriented at PA +66°. Exposure time was 3600 s in all cases. A Fe-Ne lamp was used for wavelength calibration. Using a slit width of 2″, the achieved spectral resolution (FWHM) is ≈65 km s^{-1}. The spatial resolution (FWHM), mainly determined by the seeing, is ≈1″–1″.5. The spectra were reduced using the program developed by Dr. Solf for long-slit spectroscopy (see Solf & Carsenty 1982). Bias-substraction, flat-fielding, two-dimensional wavelength calibration and sky background substraction were carried out for each spectrum. The error in radial velocities is estimated to be ≈ ±15 km s^{-1}. The internal accuracy is much better. Radial velocities quoted throughout the paper are heliocentric.

The spectra confirm the reflection and HH nature of RF and of the object departing from HL 14 respectively. Hα emission has been detected from Star 1 and HL 14 and from two faint field stars (covered by slit **a**) which are denoted Star 2 and Star 3 in Fig. 1. [S II] emission lines are also present in the spectrum of Star 2 and Star 3. Coordinates of these stars are given in Table 1. Strong Hα emission from BD+65°1637 has also been detected but the line is saturated, not permitting a detailed analysis of the line profile (see Finkenzeller & Mundt 1984). In addition, HH emission has been detected at two positions in slit **a** and the slit covering RF. Coordinates of these new HH objects, denoted by NGC 7129/HH 3 and NGC 7129/HH 4 (Fig. 1), have been estimated from the [S II] emission maximum on the spectra and are given in Table 1.

3. Discussion on individual objects

3.1. *HL 14-jet*

Figure 2 is an enlargement of the 1988 I and 1990 Hα and [S II] images around the star HL 14. Figure 3 shows isocontour plots of the 1988 and 1990 Hα and [S II] images. In Hα, the object is connected with HL 14. Firstly, the object extends ≈8″ towards the east; then it encounters reflection nebulosity and its orientation abruptly changes ≈90°, being detectable up to ≈7″ towards the south. Its angular diameter (FWHM) is ≈2″.5 (seeing corrected) and remains almost constant along the object. A similar description can be made of the [S II] image, although the object is fainter in this filter at the position where it connects with HL 14. Several condensations are embedded in the body of the

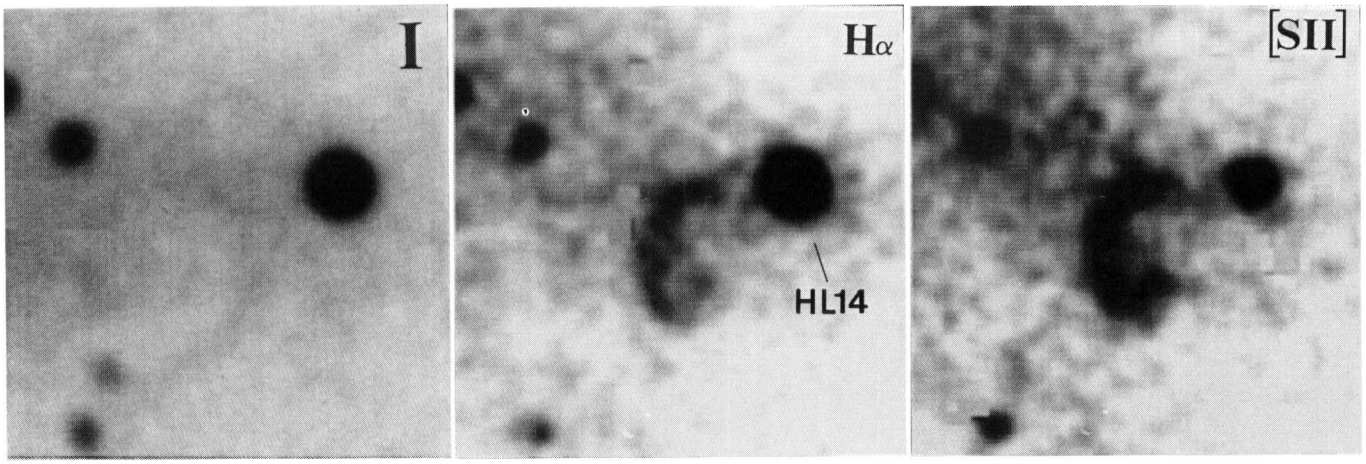

Fig. 2. 1990 Hα and [S II] images of the star HL 14 and his associated HH jet-like object. Also shown is the 1988 *I* image for comparison purposes. Field size is 25″ × 25″

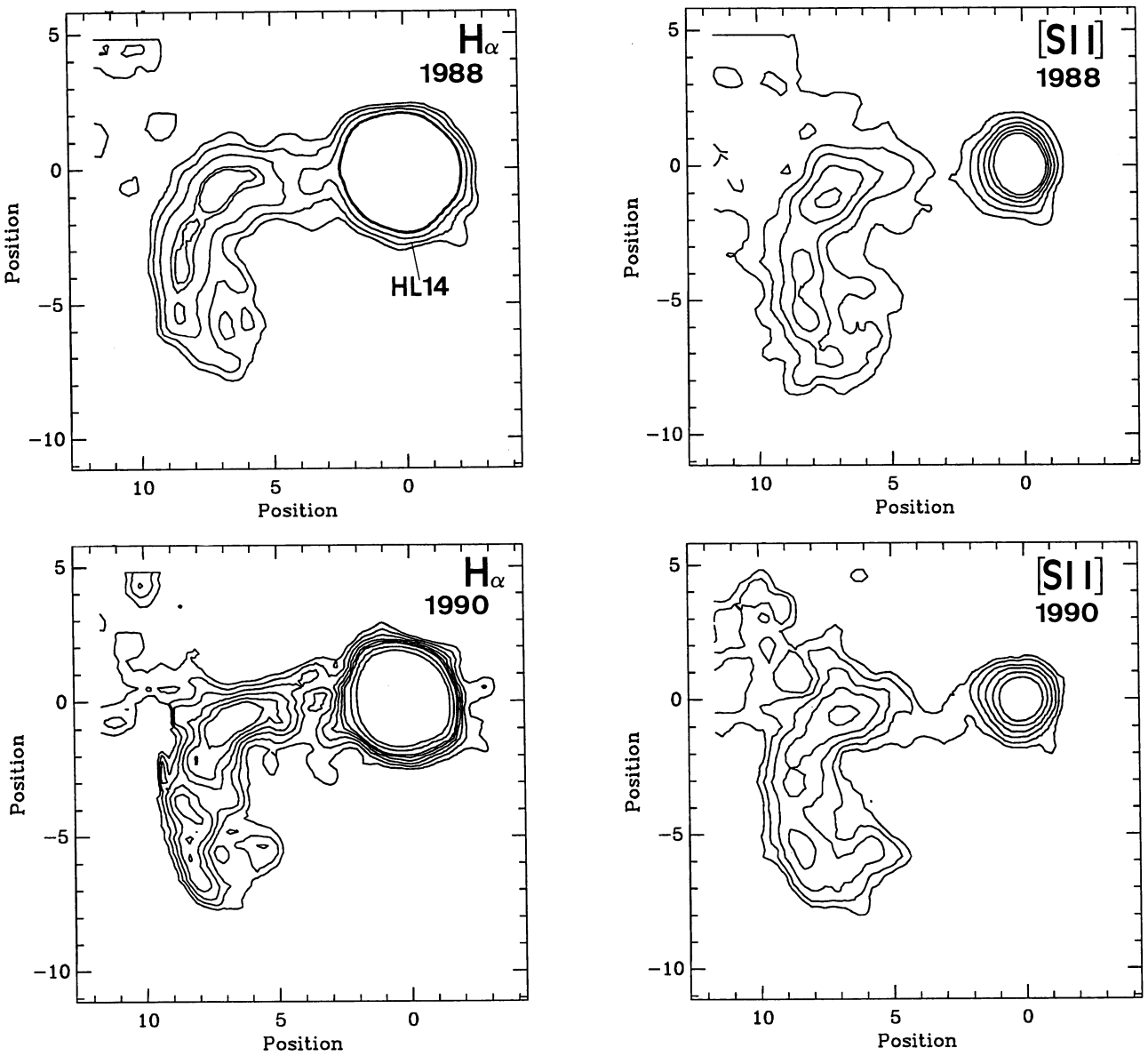

Fig. 3. Isocontour plots of the 1988 and 1990 Hα and [S II] images of the HH jet-like object associated with HL 14. The lowest contour is at 3σ level, the rest is arbitrary. Position (0,0) correspondes to the peak of HL 14. Scale in arcsec

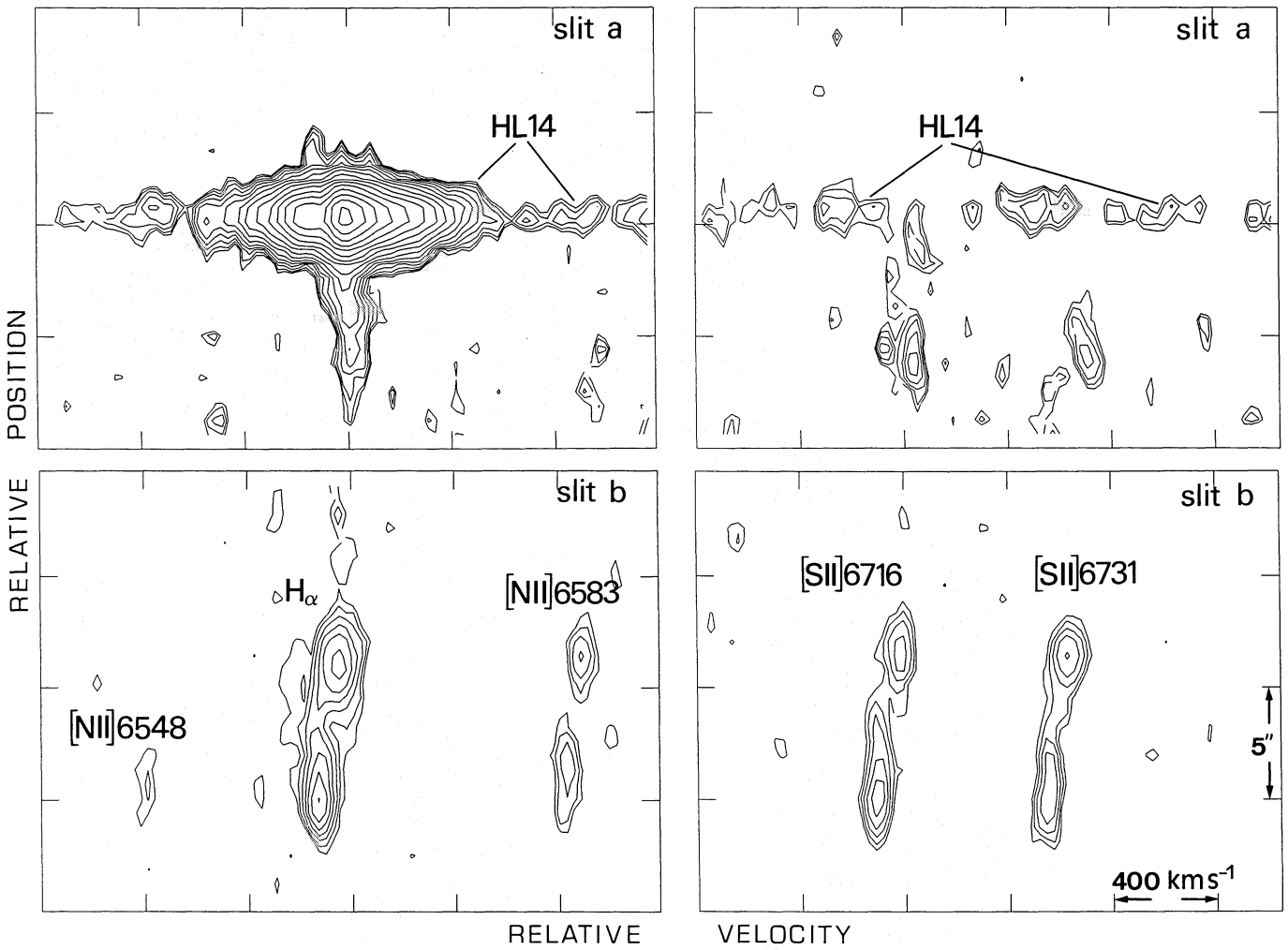

Fig. 4. Position-velocity isophotic maps of the Hα, [N II] and [S II] emission lines from the HL 14 jet-like object. Slit **a** is centered on HL 14 and oriented at PA −90°, slit **b** is centered 8″ to the east of HL 14 and oriented at PA 0°. Contours are logarithmic, separated by a factor $2^{1/2}$ in intensity

object. The strongest condensation is observed at the point where the orientation of the object changes. Changes between the Hα and [S II] images are clearly distinguished and so are those between the 1988 and 1990 images. The more striking changes occur at the position where the object connects with HL 14. In addition, the 1990 Hα image shows a weak spike to the west of HL 14, which is not observed in the 1988 Hα image.

Hα, [N II] and [S II] emission lines are detected in the spectra of the object. Figure 4 presents position-velocity (PV) isophotic maps of those lines as deduced from the spectra at slit **a** and slit **b**. Slit **a** included HL 14, from which strong Hα emission and a weak continuum is detected. Hα emission from the object can be traced up to ≈2″ to the east of HL 14 (continuum intensity peak), where it is superimposed on the prominent Hα emission from the star. A weak Hα emission feature can be recognized to the west of HL 14, extending from ≈2.″3 up to ≈4″ from HL 14. This emission feature probably corresponds to the weak spike observed in the 1990 Hα image. [N II] and [S II] emissions have not been detected within ≈4″ eastwards of HL 14 and westwards. However, it should be noted that a [S II] 6716 emission feature is observed extending from the position of HL 14 up to ≈3″ westwards. This emission feature is not observed in [S II] 6731. We suspect that the feature is not real and is probably due to an imperfect sky background subtraction. We will not consider this feature in the following analysis. At slit **b**, the emission features exhibit a similar shape, although the Hα emission seems to present two velocity components at some positions. These components are rather weak and do not allow a detailed analysis. Condensations can be recognized in the emission features at both slit **a** and slit **b**.

The radial velocity changes along the object (Fig. 4). In order to study the variations of the radial velocity a single-component gaussian line fit was performed to the spectral distribution of each emission line. Figure 5 presents the radial velocity deduced from the Hα line, as a function of

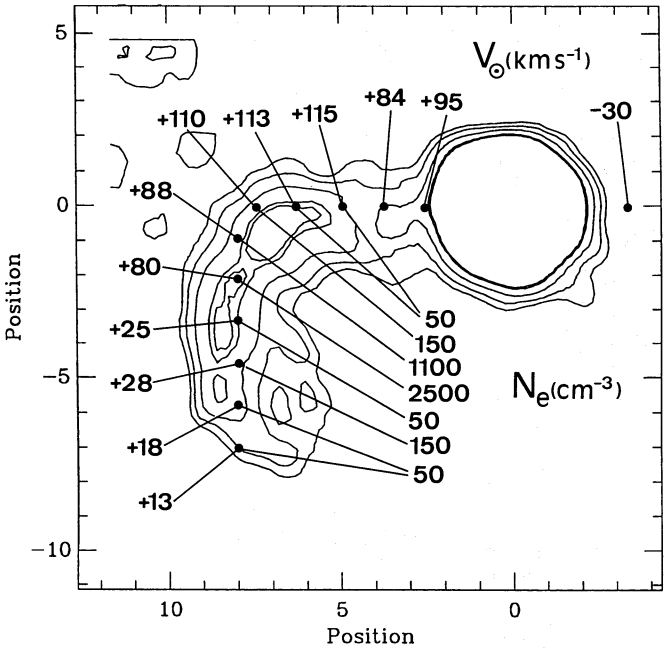

Fig. 5. Heliocentric radial velocity field and electron density deduced from the spectra of the HL 14 jet-like object, superimposed on the 1988 Hα image

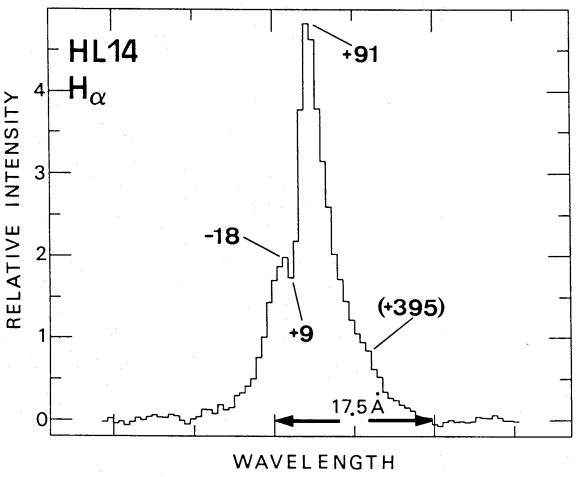

Fig. 6. Hα profile of HL 14. Heliocentric radial velocities (km s^{-1}) are indicated

the spatial position along the slits, superimposed on the 1988 Hα image of the object. The regions of the object to the east of HL 14 are redshifted whereas the weak feature to the west is blueshifted. The radial velocity increases eastwards of HL 14, reaches its maximum at $\approx 5''$ from the star and decreases across the strongest condensation ≈ 35 km s^{-1}. Then, the radial velocity abruptly decreases ≈ 60 km s^{-1} in $\approx 3''$. Southwards along the object, a slight but continuous decrease of the radial velocity can be recognized. The spectrum at slit **a** suggests that the radial velocity slightly varies in the blueshifted weak emission (Fig. 4). Radial velocities derived from the [N II] and [S II] lines agree, within $\approx \pm 5$ km s^{-1}, with those obtained from the Hα line.

The velocity dispersion, as estimated from the FWHM of the gaussian line profile, corrected for instrumental resolution, exhibits systematic variations in the object. From the Hα line, we deduced velocity dispersions of $\leqq 100$ km s^{-1} eastwards of HL 14 and ≈ 120 km s^{-1} in the strongest condensation. Remarkably, the velocity dispersion decreases up to ≈ 50 km s^{-1} southwards of the strongest condensation and remains almost constant. From the [S II] lines a velocity dispersion of ≈ 50–55 km s^{-1} is derived in the object, except in the strongest condensation where it increases up to ≈ 85–100 km s^{-1}. Velocity dispersions obtained from the [N II] lines are similar to those deduced from the [S II] lines.

The line intensity ratios systematically change in the object. The [S II] 6716+6731/Hα ratio presents values ≈ 1.4 except in the strongest condensation where the value decreases up to $\leqq 0.7$. A similar behaviour is observed in the [N II] 6583/Hα ratio, which presents values of ≈ 0.25 in the strongest condensation and ≈ 0.5 in the rest of the object. These results show that the excitation degree is significantly higher in the strongest condensation than in the rest of the object. The electron density, determined from the [S II] 6731/6716 ratio in combination with the transformation graph in Aller (1984), as a function of the spatial position, is shown in Fig. 5. The electron density in the object is very low, except to the south of the strongest condensation where it increases by a factor ≈ 50.

Figure 6 shows the Hα profile of HL 14. The profile has two emission peaks of different strength at ≈ -18 and $\approx +91$ km s^{-1}, separated by an absorption reversal which is blueshifted with respect to the centroid of the whole line. In addition, a highly redshifted component seems to be present at $\approx +395$ km s^{-1}. The wings of the Hα emission can be traced up to ≈ 1200 km s^{-1} (FWZI). Other emissions or absorption lines have not been detected in the spectrum. The observed Hα profile strongly suggests that HL 14 is a T Tauri-like young star (see e.g. Edwards et al. 1987; Appenzeller & Mundt 1989). This finding and the clear connection between the star and the HH object allow us to identify HL 14 as the exciting star of the HH object.

The morphology, the measured electron densities, radial velocities and velocity dispersions favor the idea that the object is a highly collimated, strongly bent jet-like outflow emanating from HL 14. The large bending observed in direct images suggests that the collimated outflow suffers an abrupt change of direction, which is supported by the large difference between the radial velocities observed eastwards of HL 14 and southwards along the object. The largest variation of the radial velocity is observed southwards of the strongest condensation, indicating that this condensation represents the deflection point where the outflow changes its direction. Hereafter we

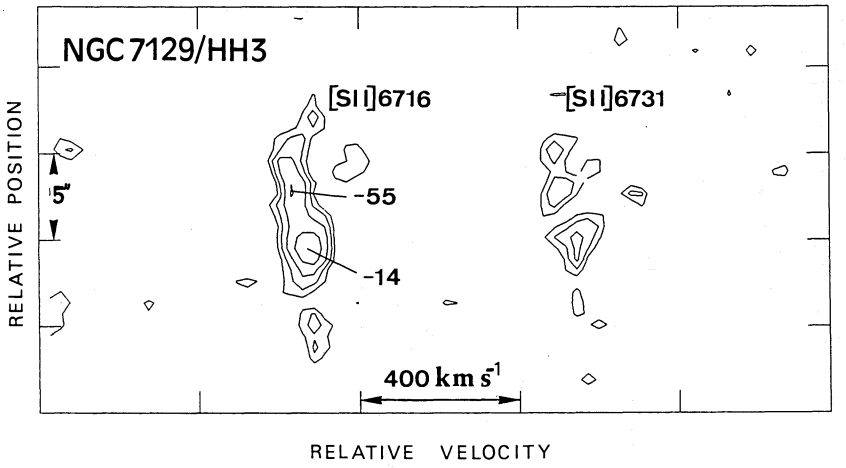

Fig. 7. Position-velocity isophotic map of the [S II] 6716, 6731 emission lines from NGC 7129/HH 3. Contours are logarithmic, separated by a factor $2^{1/2}$ in intensity. Heliocentric radial velocities (km s^{-1}) are indicated

will refer to the object as the HL 14-jet. It should be noted that, if the blueshifted component to the west of HL 14 is real, the collimated outflow from this star would be bipolar. In this case, the morphology of the two parts of the bipolar outflow (jet and counterjet) would be rather different from each other, as it is observed in several jet-counterjet systems from young stars (Mundt et al. 1991).

The deflection of the HL 14-jet could be caused by shocking of the collimated outflow with an obstacle – density enhancement or pressure gradient – in the cloud. The moderate decrease of the radial velocity accross the deflection point suggests that the outflow is decelerated before being deflected. Turbulence generated in the shock and/or increasing temperatures can account for the high velocity dispersion and high excitation observed at the deflection point. The strong condensation observed at the deflection point probably represents the site of kinetic energy dissipation in the shock. It is, however, surprising that the velocity dispersion is lower after deflection than at the deflection point. This result and the almost constant diameter of the object suggest that the outflow remains highly collimated after deflection or even that it recollimates again.

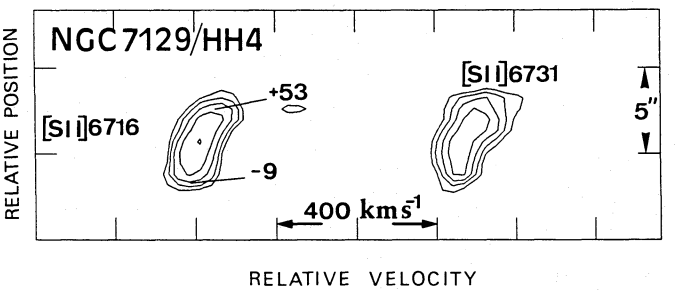

Fig. 8. Position-velocity isophotic map of the [S II] 6716, 6731 emission lines from NGC 7129/HH 4. Contours are logarithmic, separated by a factor $2^{1/2}$ in intensity. Heliocentric radial velocities (km s^{-1}) are indicated

An attractive scenario for explaining the deflection of the HL 14-jet is that the obstacle causing the deflection is related to the walls of the CO cavity or to the LkHα 234 wind. In fact, the object is redshifted and is seen projected against the body of the cavity. In addition, the images suggest that the collimated outflow encounters nebulous material at the deflection point, which may well be material in the walls of the cavity (Fig. 2). The continuous action of the expanding cavity or of the LkHα 234 wind upon the object may result in a continuous curvature of the deflected outflow towards the observer, as suggested by the decrease of the radial velocity southwards (Fig. 5). This scenario is also compatible with the temporal morphological variations observed in the object.

3.2. NGC 7129/HH 3 and NGC 7129/HH 4

Figure 7 and 8 show PV maps of the [S II] emission lines of NGC 7129/HH 3 and NGC 7129/HH 4 respectively. Radial velocities are indicated. Variations in the radial velocity are observed in both objects. NGC 7129/HH 3 is blueshifted whereas most of NGC 7129/HH 4 is redshifted. The [S II] and Hα emissions from NGC 7129/HH 3 and NGC 7129/HH 4 extend $\approx 15''$ and $\approx 6''$ respectively. Condensations can be recognized in the emission features of both objects. The mean [S II]/Hα intensity ratio is ≈ 1.3 and ≈ 0.8 in NGC 7129/HH 3 and NGC 7129/HH 4 respectively. The mean [N II] 6583/Hα intensity ratio is ≈ 0.34 in NGC 7129/HH 4, whereas no [N II] emission has been detected from NGC 7129/HH 3. These results indicate low excitation in both objects. The mean electron density presents low values of $< 100\,\mathrm{cm}^{-3}$ and $\approx 400\,\mathrm{cm}^{-3}$ in NGC 7129/HH 3 and NGC 7129/HH 4, respectively.

NGC 7129/HH 4 can be identified in the [S II] image with very faint nebulosity, whereas NGC 7129/HH 3 can not be distinguished in our images probably due to the existence of strong reflection nebulosity at its position

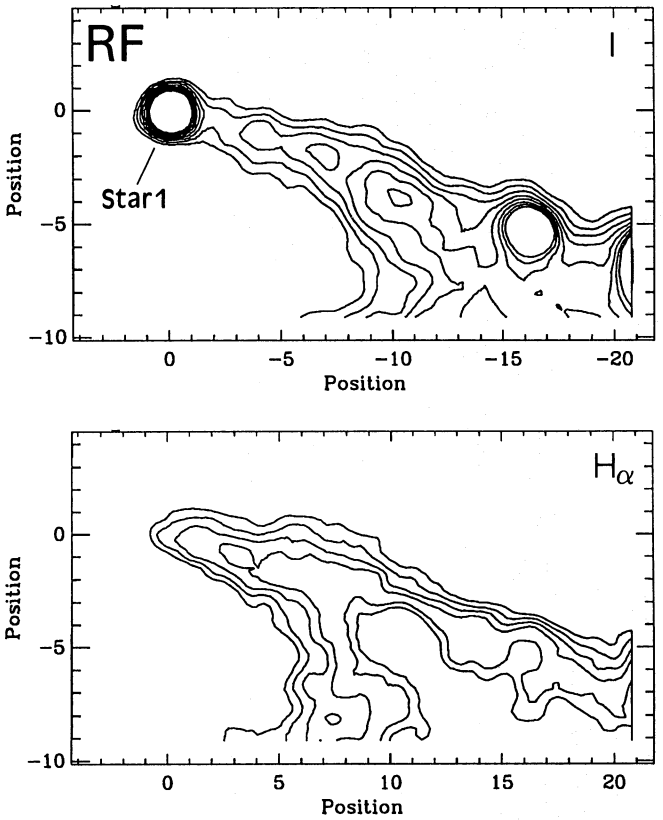

Fig. 9. 1988 *I* and 1990 Hα isocontour plots of the reflection filament RF. The lowest contour is at 3 σ level, the rest is arbitrary. Position (0, 0) corresponds to the maximum of Star 1 in the *I* image. Scale in arcsec

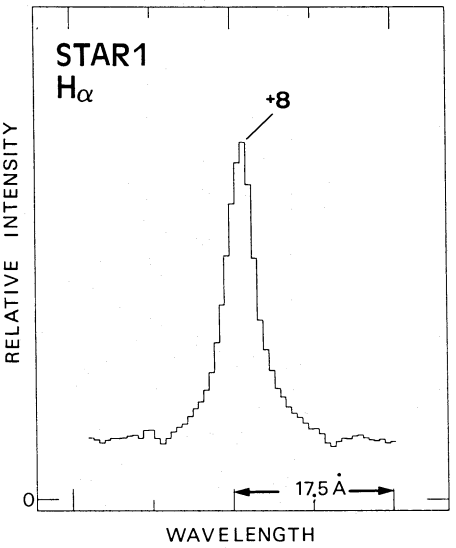

Fig. 10. Hα emission profile from Star 1. Heliocentric radial velocity (km s^{-1}) of the peak is indicated

(Fig. 1). From our data, nothing can be said about the possible exciting sources of these objects.

3.3. *RF*

Figure 9 shows 1988 *I* and 1990 Hα isocontour plots of the reflection filament RF. Grey-scale pictures of the object, including a [S II] image, can be found in Miranda et al. (1990). RF shows up as a knotty filament of $\approx 27''$ in size, extending in the east-west direction but slightly curved towards the south. Star 1 is located at the easternmost end of RF. The isocontours are much concentrated towards the star and open up with the distance, particularly in Hα. The edges of RF are bright relative to the inner parts as indicated by the sharp gradient of the outermost contours. The spectrum of RF (not shown) shows Hα emission extending $\approx 30''$ towards the southwest and $\approx 50''$ towards the northeast of Star 1. We cannot say whether the Hα emission is due to RF only or whether there is contribution of the nebulosity in which RF is embedded (Fig. 1). Nevertheless, it seems probable that the Hα emission detected towards the southwest of Star 1 does, at least partially, come from RF (see below).

The Hα emission profile of Star 1 is shown in Fig. 10. The profile presents a single symmetric peak at a radial velocity of $\approx +8$ km s^{-1}. The wings can be traced up to ≈ 800 km s^{-1}. Other emission or absorption lines are not detected in the spectrum. The data indicate that Star 1 is a young Hα emission-line star. This fact and the clear morphological connection of Star 1 and RF strongly indicate that Star 1 is the illuminating source of RF.

The results suggest that the formation of RF is related to the wind from Star 1. The elongated structure of RF suggests the existence of a focusing mechanism of the wind from Star 1, e.g. a disk. It is, however, noteworthy that RF traces the northern edge of the CO cavity, and that molecular material moving along the walls of the cavity has been observed (Bertout 1987). Thus, an interesting possibility is that this moving material is pushing the wind from Star 1 and directing it along the walls of the cavity which probably represents the direction of less resistance.

3.4. *Star 2 and Star 3*

Figures 11 and 12 present the spectra of Star 2 and Star 3 respectively. In both cases, Hα and [S II] emission lines are detected. Hα radial velocities are indicated in the figures. The Hα profile of Star 2 presents two emission peaks at ≈ -104 and $\approx +130$ km s^{-1}, separated by an absorption reversal at $\approx +44$ km s^{-1}, which is redshifted with respect to the centroid of the line. The [S II] emission lines present two velocity components at ≈ -6 and -165 km s^{-1} (average of both [S II] lines). The Li I 6707 absorption line seems to be present, although this must be confirmed by new observations. Star 3 represents an asymmetric Hα profile consisting of two components at ≈ -169 and

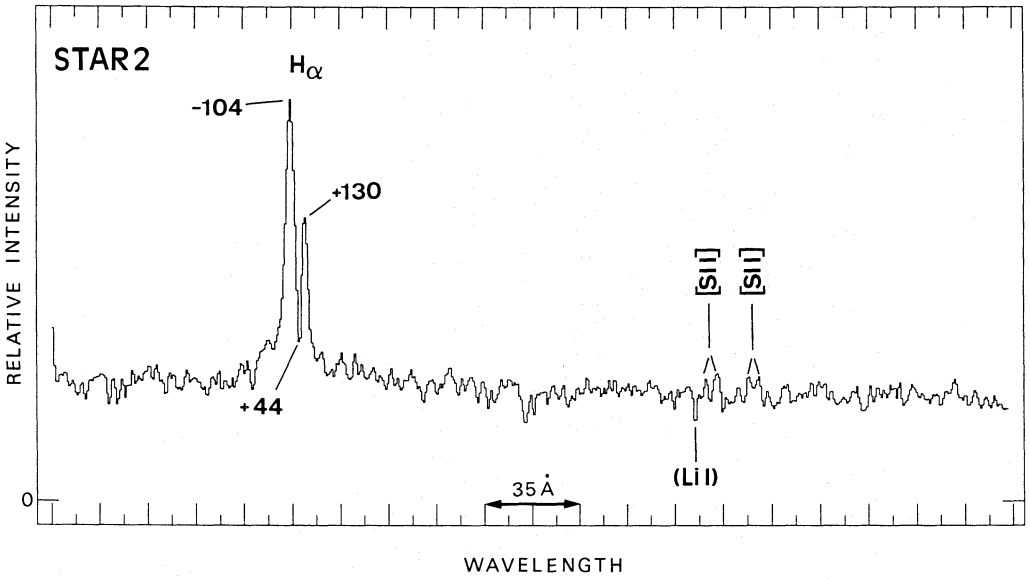

Fig. 11. Spectrum of Star 2 between 6470–6820 Å. Hα heliocentric radial velocities (km s^{-1}) are indicated

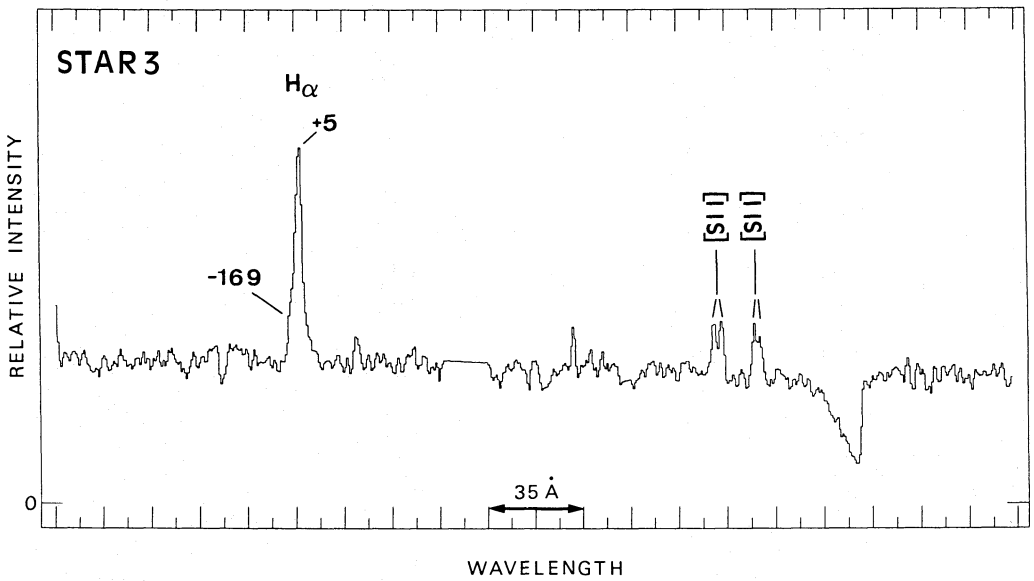

Fig. 12. Spectrum of Star 3 between 6470–6820 Å. Hα heliocentric radial velocities (km s^{-1}) are indicated

$\approx +5$ km s^{-1}. The wings of the Hα emission can be traced up to $\geqq 420$ km s^{-1}. The [S II] emission lines present two components at ≈ -16 and -120 km s^{-1}. The spectra indicate that Stars 2 and 3 are T Tauri-like stars.

4. Conclusions

The main conclusions from this work can be summarized as follows:

1. CCD images of the central part of NGC 7129 reveal the existence of many reflection filaments which seem to trace the boundaries of the CO cavity associated with the Herbig Ae/Be star LkHα 234.

2. Three new T Tauri-like young stars have been identified. The spectra confirm that the star HL 14 is also a T Tauri-like star. These results increase the number of known low-mass pre-main-sequence stars in NGC 7129.

3. One of the new young stars seems to illuminate an elongated reflection filament RF which traces the northern edge of the CO cavity in NGC 7129.

4. Five new Herbig-Haro objects have been identified either in direct images or through their emission in the spectra.

5. One of the HH objects probably represents a highly collimated, strongly bent jet-like object emanating from HL 14. The large and systematic variations of the radial velocity, velocity dispersion, electron density and excitation observed in the object favor the idea that the collimated outflow encounters an obstacle in the cloud and experiments a large deflection. The obstacle causing the deflection could be related to the walls of the molecular cavity associated with LkHα 234 or to the wind from this star.

Acknowledgements. The Calar Alto Observatory is operated jointly by the Max-Planck-Institut für Astronomie (Heidelberg) and the Spanish Comisión Nacional de Astronomía. We thank the Calar Alto staff for their help during the observations. The spectra were reduced during a stay of L.F.M. at the MPIA. He is grateful to J. Solf for his program and to Prof. Elsässer for making the stay possible. Comments and suggestions by J. Eislöffel, R. Mundt and J. Solf are acknowledged. This work has been supported in part by Spanish Grants DGICYT PB 87-0167 and PB 90-0387.

References

Aller L.H., 1984, Physics of Thermal Gaseous Nebulae. Reidel, Dordrecht
Appenzeller I., Mundt R., 1989, A&AR 1, 291
Bechis K.P., Harvey P.M., Murray F.C., Hoffman W.F., 1978, ApJ 226, 439
Bertout C., 1987, Circumstellar Matter, IAU Symp. No. 122, Appenzeller I., Jordan C. (eds.). Reidel, Dordrecht, p. 23
Cesarsky C.J., Cesarsky D.A., Churchwell E., Lequeux J., 1978, A&A 68, 33
Dent W.R.F., Sandell G., Duncan W.D., Robson E.I., 1989, MNRAS 238, 1497
Edwards S., Snell R.L., 1983, ApJ 270, 605
Edwards S., Cabrit S., Strom S.E., Heyer I., Strom K.M., Anderson E., 1987, ApJ 321, 473
Eiroa C., Gómez de Castro A.I., Miranda L.F., 1992, A&AS 92, 721
Finkenzeller U., Mundt R., 1984, A&AS 55, 109
Goodrich R.W., 1986, AJ 92, 885
Güsten R., Marcaide J.M., 1986, A&A 164, 342
Hartigan P., Lada C.J., 1985, ApJS 59, 383 (HL)
Harvey P.M., Wilking B.A., Joy M., 1984, ApJ 278, 156
Herbig G.H., 1960, ApJS 4, 337
Miranda L.F., Eiroa C., Gómez de Castro A.I., 1990, Ap&SS 171, 223
Mundt R., Ray T.P., Raga A.C., 1991, A&A 252, 740
Racine R., 1968, AJ 73, 233
Ray T.P., Poetzel R., Solf J., Mundt R., 1990, ApJ 357, L45
Reipurth B., Graham J.A., 1988, A&A 202, 219
Rodríguez L.F., Moran J.M., Ho P.T., Gottlieb E.W., 1980, ApJ 235, 845
Sandell G., Olofsson H., 1981, A&A 99, 80
Shu F.H., Adams F.C., Lizano S., 1987, ARA&A 25, 23
Solf J., Carsenty U., 1982, A&A 113, 142
Strom K.M., Strom S.E., Wolff S.C., Morgan J., Wenz M., 1986, ApJS 62, 39
Strom S.E., Grasdalen G.L., Strom K.M., 1974, ApJ 191, 11